

pubs.acs.org/Macromolecules Article

Controlled Degradation of Cast and 3-D Printed Photocurable Thioester Networks via Thiol—Thioester Exchange

Juan J. Hernandez, Adam L. Dobson, Benjamin J. Carberry, Alexa S. Kuenstler, Parag K. Shah, Kristi S. Anseth, Timothy J. White, and Christopher N. Bowman*



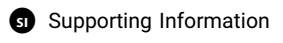
Cite This: Macromolecules 2022, 55, 1376-1385



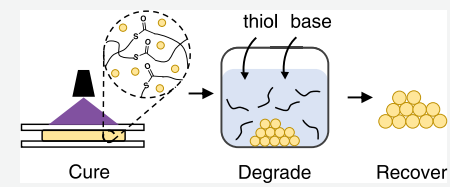
ACCESS I

Metrics & More





ABSTRACT: This work examined and quantitatively predicted the degradation of thioester-containing networks facilitated by base-catalyzed thiol—thioester exchange. A statistical model was developed that incorporated polymer structure, thiol—thioester exchange reaction kinetics, and mass gain resulting from dynamic bond exchange, and this model was compared to mass loss studies. Experimental results matched model predictions, showing that degradation times could be controlled from 2.5 to 12 h with optimal conditions by varying the free thiol butyl 3-mercaptopropionate concentration



from 0.0 to 4.9 M and the base-catalyst triethylamine molar ratio from 0 to 40 mol %. Furthermore, thioester-based composite materials were formed by stereolithography (SLA) three dimensional (3-D) printing and subsequently degraded, achieving 91% recovery of the composite filler. This work provides insight into thioester-facilitated degradation and its future use in selective material release or encapsulated filler recovery applications.

1. INTRODUCTION

In recent years, waste from slowly degrading polymers has driven the need to consider the holistic lifecycle of manufactured plastics. Polymers that cannot degrade rapidly or be recycled pollute the environment, leading to an increased focus on designing multiuse or on-demand degradable plastics. Polymer composites that cannot degrade must be scrapped, leading to the loss of both specially synthesized chemical components and valuable fillers used to make these composites.²

One subset of polymers, thermosets, are particularly difficult to degrade but have advantageous material properties. Thermosets are composed of covalent chemical cross-links that enable dimensional stability, solvent resistance, and temperature resistance. However, the nonreconfigurability of these permanent cross-links limits recyclability or reuse and further inhibits degradation. Covalent adaptable networks (CANs) offer an effective way to reuse thermoset polymers by having cross-links with triggerable, dynamic bonds.³ Rearrangement of these dynamic bonds allows reprocessing of thermosets, and different dynamic chemistries use different stimuli to induce network rearrangement, for example, by exposure to heat or light.4 Past work has shown that CANs enable thermoset degradation, 5-9 yet these studies are often empirical, and it remains a challenge to quantitatively predict degradation behavior, limiting their application in larger-scale processes such as stereolithography (SLA) additive manufacturing. SLA uses light to cure liquid monomers layer by layer to form a three dimensional (3-D) object. While a variety of dynamic chemistries, such as transesterification, 10 disulfide metathesis, 11,12 and trithiocarbonate addition-fragmentation,¹³ have been SLA 3-D printed, little work has been done to explore the degradation process of these printed CAN-based polymers.

Degradation in CANs refers to the permanent cleavage of cross-links in a network, which leads to the formation of detached monomers and a reduction in mass as the increasing sol fraction comprised of monomers and oligomers leaves the network.¹⁴ This degradation process has two limiting extremes: surface and bulk degradation. 15 Surface degradation is a diffusion-limited process where cross-links are cleaved only on the surface of a bulk polymeric object, gradually shrinking the material from the outside until the entire network dissolves into solution. Conversely, bulk degradation is a reactionlimited process where cross-links are cleaved throughout the entire polymer network simultaneously until the reverse gelation point is reached and the material depolymerizes and fully dissolves into solution. 15 Often, degradation of a polymer network is a combination of both surface and bulk mechanisms.

Of the various dynamic chemistries, degradation studies on thioester-containing networks offer a wider understanding of network architectures due to thioesters being compatible with the existing thiol-X chemistries. Dynamic bond rearrangement in thioester-containing CANs comes from the thiol—thioester

Received: November 29, 2021 Revised: January 21, 2022 Published: February 4, 2022





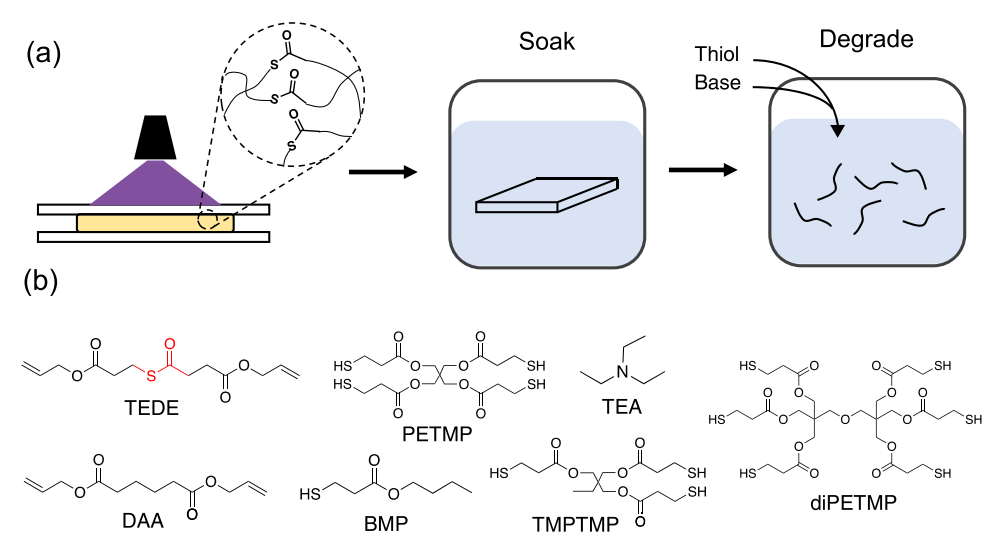


Figure 1. Addition of excess thiol and base catalyst triggers the degradation of thioester-containing thermosets via thiol—thioester exchange. (a) Thioester-containing networks were photocured via thiol—ene combination, swelled in acetone, and degraded by exposure to thiol and base. (b) Monomers, free thiol, and base catalyst used to create networks and trigger thiol—thioester exchange.

exchange reaction, which may occur through either a base- or a nucleophile-mediated pathway. While other thiol-based dynamic chemistries have been used to create dynamic networks, such as Meldrum's acid systems ^{17,18} and thiol—yne systems, ^{19,20} thiol—thioester exchange is attractive due to its highly selective reactivity with thiols, efficiency with mild bases, stability in aqueous solutions, and inherent biocompatibility as a common biosynthetic pathway. ^{16,21–23} While past work has shown that thioester networks degrade efficiently (Figure 1) and may be SLA 3-D printed, ²⁴ the process and time scale for degradation of these structures have yet to be investigated.

Past studies on the degradation process of other dynamic chemistries offer guidance on how to study thioester-based degradation. In ester cross-linked materials, mass loss resulting from transesterification-based CAN degradation is well described by models that combine surface and bulk degradation. 25-27 Recent work on boronic ester CAN degradation similarly created a surface degradation model that also matched mass loss studies.²⁸ However, a bulk degradation model for CANs is missing, and this model would more accurately capture the relevant degradation processes of CANs with thinner cross-sectional areas, such as those formed in 3-D printed parts. Past work on understanding bulk degradation of thermosets has focused on studying the degradation of hydrogels, 5,29-33 and while these analyses provide insightful models, they are not applicable to more hydrophobic or more cross-linked bulk CANs, which may experience significantly reduced swelling. To this end, a bulk degradation model of thioester-based CANs would both investigate the degradation processes particular to thiolthioester exchange and also widen the scope of degradation models applicable to CAN chemistries.

This paper sought to investigate the degradation process and time scale that thiol—thioester exchange enables in cast and 3-D printed networks. As such, a statistical kinetic model for bulk degradation of thioester networks was generated, which combined the thiol—thioester exchange reaction kinetics, mass gain resulting from thiol—thioester exchange, and the structure of the polymer network being degraded. Mass loss experiments verified model predictions for how the concentration of free thiol, relative mol percent of base catalyst, and

monomer functionality all impacted mass loss rates. Lastly, 3-D printed and degraded thioester composites matched model predictions for the degradation time of 3-D printed samples and showed the effectiveness of using thioester degradation to selectively recover composite fillers. The understanding of thiol—thioester-facilitated degradation gained in this work enables the implementation of degradable thioester systems for recycling and selective material recovery applications in additive manufacturing specifically and in composite materials generally.

2. MATERIALS AND EXPERIMENTAL METHODS

2.1. Materials. A previously reported procedure was used to synthesize the thioester monomer TEDE.³⁴ All other materials used were purchased commercially and used without further purification. 3-Mercaptopropionic acid (3-MPA), allyl alcohol (AA), butyl 3-mercaptopropionate (BMP), trimethylpropane Tris(3-mercaptopropionate) (TMPTMP), p-toluenesulfonic acid (pTsOH), pentaery-thritol tetrakis(3-mercaptopropionate) (PETMP), and cross-linked poly(styrene-co-divinylbenzene) microspheres (6–10 um) were purchased from Sigma-Aldrich. Diallyl adipate (DAA) and succinic anhydride (SA) were purchased from TCI Chemicals. 4-Dimethylamino-pyridine (DMAP) was purchased from Oakwood Chemical, dipentaerythritol hexakis(3-mercaptopropionate) (diPETMP) was obtained from Bruno Bock Chemische Fabric, and Irgacure 819 (1819) was purchased from IGM Resins.

2.2. Thin Film Preparation and Degradation. To prepare thioester films, one thiol and one ene monomer were combined with I819 and pyrogallol in a molar ratio of 1 thiol: 1 ene: 0.5 wt % I819: 0.06 wt % pyrogallol, loaded between glass slides spaced 100 μ m apart, and irradiated to complete conversion (405 nm, 30 mW/cm², 5 min). Samples were then trimmed to a length and width of 25 mm, with an average weight of 100 mg, and used for further experiments.

The initial mass of each film was recorded, $m_{\rm o}$, and then samples were allowed to swell in a solution of BMP and acetone overnight, with the concentration of BMP set by the degradation conditions. Films were then transferred to a constructed apparatus composed of a covered 100×50 mm Pyrex Petri dish, a stir bar spun at 400 RPM, and a steel grid, which let degradation solution flow above and below the films (Figure S3 in the SI). TEA was added to initiate degradation, and then films were removed at specific times and patted dry with a Kimwipe. Films were then soaked in acetone overnight, dried in a vacuum oven at 50 °C for 24 h, and weighed again to measure the final dry mass, $m_{\rm final}$. Experimental mass loss was calculated by

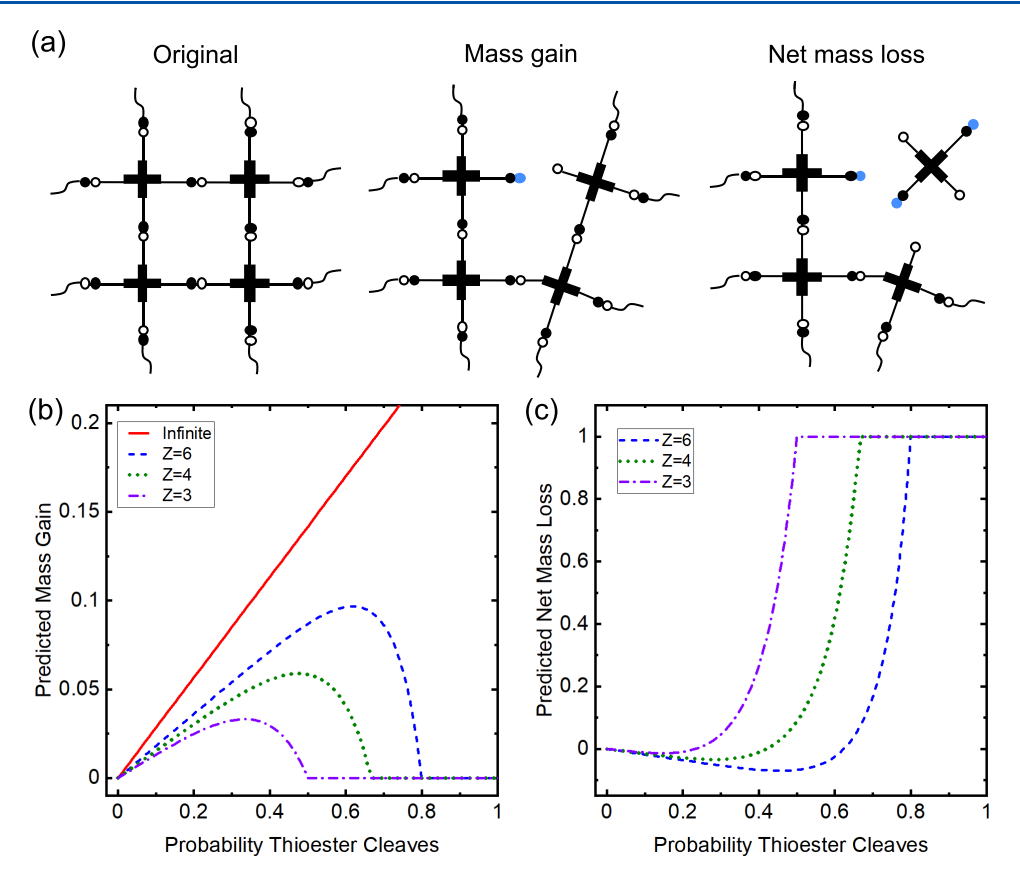


Figure 2. Degradation of thioester-containing networks is predicted to proceed first through a small amount of mass gain and then through net mass loss based on the derived model. (a) Thioesters (black circles) and thiols (white circles) underwent exchange with free thiol (blue circles). Net mass loss was achieved when all bonds of a repeat unit were cleaved (right). (b) Plot comparing the predicted mass gain from thiol—thioester exchange versus the probability a thioester cross-link cleaves, as was calculated by eq 9. (c) Plot comparing the predicted net mass loss from thiol—thioester exchange versus the probability a thioester cross-link cleaves based on eq 10.

$$ML_{exp} = \frac{m_{o} - m_{final}}{m_{o}} \tag{1}$$

2.3. 3-D Printing and Filler Recovery. Samples were 3-D printed on a Prusa SL1 masked-SLA 3-D printer, washed with dichloromethane, and air-dried for 30 min. Printed resins contained a molar ratio of 1 thiol: 1 ene: 0.5 wt % I819: 0.06 wt %. Thioester composites contained 80 wt % resin and 20 wt % poly(styrene-co-divinylbenzene) microspheres. Exposure times and E_cD_p values for 3-D printed parts are listed in Table S1.

3-D printed composites were placed in a solution of 2M BMP and 30 mol % TEA in acetone and allowed to stir overnight to recover the microspheres. Acetone was added at twice the volume of the initial solution, and the mixture was centrifuged at 1000 RPM for 2 min. The settled microspheres were then redispersed in pure acetone, centrifuged again at 1000 RPM for 2 min, and dried in a vacuum oven at 50 $^{\circ}\mathrm{C}$ for 24 h.

2.4. Dynamic Mechanical Analysis. An RSA-G2, from TI Instruments, was used for dynamic mechanical analysis (DMA). Samples were heated from -50 °C to 50 °C, with a ramp rate of 3 °C/min and a frequency of 1 Hz. Samples were run in tension with a strain of 0.03% and a preload force of 0.34 N. The $T_{\rm g}$ was determined as the peak of the tan delta curve. The molecular weight between cross-links, $M_{\rm cl}$ was calculated from DMA data via

$$M_{\rm c} = \frac{3\rho R T_{\rm min}}{E_{\rm r,min}} \tag{2}$$

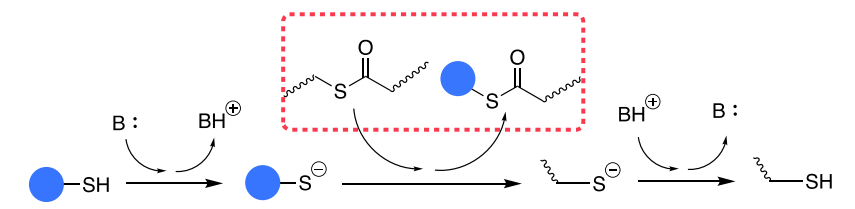
where ρ stands for polymer density and was assumed to be constant at 1100 kg/m³, R stands for the universal gas constant, $E_{\rm r,min}$ stands for the minimum storage modulus value just as the polymer enters the

rubbery plateau, and $T_{\rm min}$ stands for the temperature in Kelvin where $E_{\rm r,min}$ is reached. 35

2.5. Model Development. Modeling bulk degradation of an ideal step-growth polymer network containing thioester linkages required examination of the step-growth network structure and the reaction kinetics of thiol-thioester exchange. The approach used here was modified from Rydholm et al., 32 which, in turn, was based on stepgrowth network formation equations first proposed by Macosko and Miller.³⁶ This model was derived with four primary assumptions: (i) the polymers under consideration were ideal networks; (ii) the reaction rate constant for the thiol-thioester exchange remained constant throughout the degrading process; (iii) cleaved segments diffused nearly immediately out of the thioester network; and (iv) no further thiol-thioester exchange reactions need be considered in cleaved segments because these segments rapidly diffused out of the network and did not have time for additional thiol-thioester exchange. These assumptions will not hold for all networks and may be of interest to explore in future studies. Past work suggests that cyclization occurs to varying extents,³² reaction rate constants may depend on temperature and other conversion-dependent network features, 26 networks with larger values of M_c will cleave into large oligomers with significant diffusion times, 37 and lastly, networks containing multiple degradable thioester units between cross-links will increase the likelihood of secondary thiol-thioester exchange reactions that may reattach segments prior to their release.21

2.5.1. Structure Component of Model. For an ideal step-growth network with monomer functionality Z, each arm of the multifunctional monomer unit is detached from or attached to an infinite network with probability y or 1-y, respectively. Detachment from the network can occur in two ways. The first is via cleavage of the thioester bond from an adjacent multifunctional monomer unit

Scheme 1. Base-Catalyzed Thiol—Thioester Exchange Swaps the Group Attached to a Free Thiol with the Group Attached to a Thioester and Thioester.



^aIn this work, the thioester groups were initially connected to the network and the exchange resulted in dangling ends (highlighted box).

through the thiol—thioester exchange reaction. This occurs with a probability *P*, the fraction of thioester bonds that have been cleaved. The second is via detachment of an adjacent monomer unit. Given that the connecting thioester bond is not cleaved, an arm can be detached from the infinite network if the neighboring multifunctional monomer unit has all its remaining arms detached from the network. This provides an equation for the probability of arm detachment as a function of the thiol—thioester exchange and network connectivity

$$y = P + (1 - P)y^{Z-1}$$
 (3)

where y is the probability that an arm of a multifunctional monomer unit is detached from the network; P is the probability that a thioester bond has cleaved, which is dictated by the thiol—thioester exchange kinetics; and Z is the number of functional groups on a monomer. Recognizing that y=1 is always a solution to eq 3, the factor y-1 can be removed from the equation, leaving a general equation in y, for Z>2

$$\sum_{k=1}^{Z-2} y^k = \frac{P}{1 - P} \tag{4}$$

The general equation predicts a critical value for $P\left(P_{c}\right)$ above which y=1 and the polymer network shifts from an infinite network to finite, soluble components. This value of P_{c} corresponds to the point of reverse gelation, given by

$$P_{\rm c} = \frac{Z - 2}{Z - 1} \tag{5}$$

The value of P_c from eq 5 agrees exactly with the Flory prediction for reverse gelation of a stoichiometric reaction of monomers with functionality Z (SI Section 2.6).³⁸

2.5.2. Mass Loss from y, P, and Network Properties. Maximum percent mass loss in such a system is given by the sum of the mass fractions of all degradable units in the network multiplied by the fraction of those units that have separated from the network

$$ML_{max} = \sum_{i} W_{i}F_{i}$$
 (6)

where W_i is the mass fraction of the degradable component i in the network and F_i is the fraction of those components that have separated from the network. In the ideal step-growth network examined, the entire mass of the network consists of one type of repeat unit: multifunctional monomer units with thioester linkers between them. This results in the mass fraction of these units in the network to be one or $W_i = 1$. The fraction of these multifunctional monomer units that have detached from the infinite network is the fraction of units that have all arms, i.e., Z number of arms, detached. This results in a fractional mass loss equation for an ideal step-growth network

$$ML_{max} = y^{Z}$$
 (7)

where y^Z represents F_y the proportion of multifunctional monomer units that have detached from the network.

Early in the degradation process, however, mass gain as a function of the degrading thiol molecular weight is expected. As thioesters become cleaved, there is a net mass gain of the excess monofunctional thiol used for degradation as these molecules add to the network (Figure 2a, middle). This mass adds to the overall network until the arm containing that thioester is detached from the network (Figure 2a, right). To account for this effect, a parameter q is defined to be the fraction of thioesters that have been cleaved but are still attached to the network, where

$$q = \frac{1}{2}P(1 - y^{Z-1}) \tag{8}$$

This relationship represents the probability that a thioester has cleaved (P) and that at least one of the other arms of the multifunctional monomer unit remains attached. The prefactor 1/2 is necessary because only half of the dangling ends formed via thioester cleavage contributes to the mass gain. A detailed derivation for eq 8 can be found in the Supporting Information Section 2.4.

From q, the total number of thioester bonds that have been cleaved but are still attached to the network can be calculated from the stoichiometry of network formation and the assumption that one molecule of excess thiol used for degradation reacts with one thioester bond. Combining the expression for q and knowledge of network stoichiometry provides the following equation for fractional mass gain

$$MG = \frac{ZP(1 - y^{Z-1})MW_{SH}}{2(2 MW_M + Z \cdot MW_{diene})}$$
(9)

where MG is the fractional mass gain, MW_{SH} is the molecular weight of the excess monofunctional thiol, MW_{diene} is the molecular weight of the thioester-containing diene, and MW_{M} is the molecular weight of the multifunctional monomer (SI Section 2.5). Combining the mass gain from eq 9 with the mass loss from eq 7 gives an expression for the net fractional mass loss

$$ML_{Model} = y^{z} - \frac{ZP(1 - y^{Z-1})MW_{SH}}{2(2 MW_{M} + Z \cdot MW_{diene})}$$
(10)

2.5.3. Kinetic Component of Model. The kinetics of the thiol—thioester exchange reaction drive the degradation rate. As shown in Scheme 1, when thioesters are initially linked to a network, the exchange forms a new thioester with a dangling end, thereby reducing the number of cross-links.

By setting the initial conditions of the thiol—thioester exchange to use a large excess of free thiol and base catalyst, the exchange can be tuned to behave as a pseudo-first-order reaction. The initial concentration of free thiol and base governs the formation of unlinked thiolate (Scheme 1, left). If the unlinked thiolate consumed by the thiol—thioester exchange is minimal (Scheme 1, middle), then the formation of unlinked thiolate can be considered an acid—base reaction in equilibrium. Knowing the initial concentration of free thiol and base catalyst and the pKa of each component, the concentration of thiolate created is calculated using

$$10^{\Delta_{\text{pKa}}} = \frac{[\text{S}^-]^2}{([\text{SH}]_0 - [\text{S}^-])([\text{B}]_0 - [\text{S}^-])}$$
(11)

where $\Delta p K_a$ stands for the difference in $p K_a$ values between the free thiol and base, $[SH]_0$ stands for the initial concentration of free thiol, $[B]_0$ stands for the initial concentration of base, and $[S^-]$ stands for

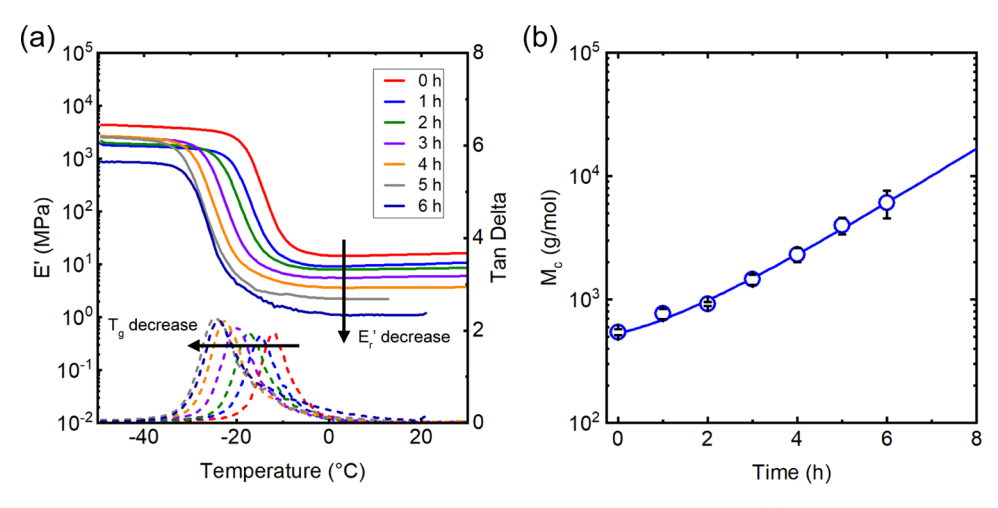


Figure 3. T_g and M_c measurements suggested that thioester networks underwent bulk degradation. (a) Plot comparing storage modulus and tan delta with temperature, repeated for various film degradation times, shows that increased degradation time lowered T_g and E_r' of films, which was typical of bulk degradation. (b) Plot comparing M_c with film degradation time shows that model prediction (line) matched experimental data (markers) well. The model prediction used eq S4 in the SI for a Z=4 network where rate constant $k=0.0051\pm0.0001~{\rm M}^{-1}~{\rm min}^{-1}$ including standard error.

the concentration of unlinked thiolate. This produces a quadratic equation in $[S^-]$ that is readily solved.

The initial concentration of unlinked thiolate in all experiments of this study was more than 200× the initial concentration of thioesters linked to the network. As such, the consumption of the unlinked thiolate by the thiol—thioester exchange was minimal and eq 11 applied. Furthermore, the large excess of unlinked thiolate drove thiol—thioester exchange toward the reaction products consistent with Le Chatelier's principle. Thus, while the thiol—thioester exchange was a second-order reaction, the effectively constant concentration of unlinked thiolate allowed the exchange to be treated as a pseudo-first-order reaction modeled by

$$[TE] = [TE]_0 e^{-k[S^-]t}$$
(12)

where [TE] refers to the current concentration of thioesters linked to the network and [TE]₀ refers to the initial concentration of thioesters linked to the network.

The network structure and kinetics portions of the model come together by relating the probability of cleaving a random thioester cross-link, *P*, to the concentration of linked thioesters via

$$P = \frac{[\text{TE}]_0 - [\text{TE}]}{[\text{TE}]_0} = 1 - e^{-k[S^-]t}$$
(13)

Equation 13 uses eq 12 to relate the probability P to the second-order rate constant k, the unlinked thiolate concentration $[S^-]$, and the time t. Combining eqs 4, 10, and 13 gives a direct prediction for how the mass of a thioester-containing polymer will decrease with time due to thiol—thioester exchange.

3. RESULTS AND DISCUSSION

3.1. Model Results for Mass Loss. The derived model provides insight into how network structure and reaction kinetics impact bulk degradation of thioester networks. Inspection of eq 10 showed that Z, the functionality of the thiol monomer and a vital part of the network structure, impacts the net mass loss and mass gain. For Z=2, a polymer consists entirely of linear polymer chains. In this case, y=1 for all values of P, and the predicted net fractional mass loss is 1, indicating that a cross-linked network is never formed. On the other extreme, as $Z \to \infty$, the value for net mass loss approaches $-\frac{PMW_{SH}}{2 \text{ MW}_{diene}}$ for P < 1. This value is a function of excess thiol molecular weight (from MW_{SH}), the number of

thioester units in the network (from MW_{diene}), and the time allowed for degradation (from P). The negative sign indicates that only mass gain is expected in such a system, as no monomer unit can leave until all thioester groups have been cleaved.

Figure 2b,c uses model systems of TMPTMP (Z=3), PETMP (Z=4), and diPETMP (Z=6), with BMP as the excess monothiol and TEDE as the thioester-containing diene to show the extreme and intermediate cases for Z. For the less cross-linked system (Z=3), mass gain was predicted but was nearly balanced by mass loss (Figure 2c). For the more highly cross-linked systems (Z=4 and 6), however, mass gain had a significant overall effect. This outcome arose because a much higher P, which corresponded to a longer degradation time, was required before units could be freed from the network. The result of this was an approximately 3 and 7% net gain in mass for Z=4 and 6, respectively, before mass loss could counteract the effect of thiol addition to the network.

3.2. Verification of Bulk Degradation. To ensure that the thioester networks experimentally studied in this work underwent bulk rather than surface degradation, the molecular weight between cross-links, M_c , and glass-transition temperature, T_g , of a model network was probed by DMA throughout the degradation process. Bulk degradation leads to a decrease in network connectivity throughout the entire polymer network, and as such, all properties that depend on network connectivity, such as M_c and $T_{g'}$ shift during degradation.³⁹ Figure 3 shows that as degradation proceeded in photocured TEDE-PETMP films soaked in 2M BMP and 30 mol % TEA degrading solution, $T_{\rm g}$ dropped and $M_{\rm c}$ increased in ways that were characteristic of films experiencing bulk degradation. Figure 3a shows that with increasing degradation time, T_g decreased from -12 to -26 °C, and the rubbery plateau modulus decreased from 14 to 1.5 MPa. Figure 3b shows that experimental data for M_c , as was calculated by eq 2, increased with degradation time and matched bulk degradation model predictions for M_c (eqs S4 and S5 in the SI).

Comparisons of characteristic reaction and diffusion times and mass swelling ratio of thin films also supported the claim that these thioester networks underwent bulk degradation. The characteristic reaction time was ≈ 100 times larger than

diffusion time (420 and 5 min, respectively), which suggested a reaction-limited process (SI Section 2.3). The mass swelling ratio of the thin films increased up to 20 during degradation, which also suggested the cleavage of cross-links within the polymer network as is characteristic of bulk degradation (Figure S2 in the SI).

3.3. Verification of Model. To validate the derived bulk degradation model, the predicted mass loss as a function of three process variables was compared to the experiment: the initial free thiol concentration, the initial molar ratio of thiol to base, and the monomer functionality, Z. Changing the multifunctional thiol monomer used to create these networks allowed Z to range from 3 to 6 (Figure 1b).

3.3.1. Free Thiol Concentration. As the initial concentration of free thiol increased, so too did the rate of mass loss. The data in Figure 4 show how mass loss changed as a function of

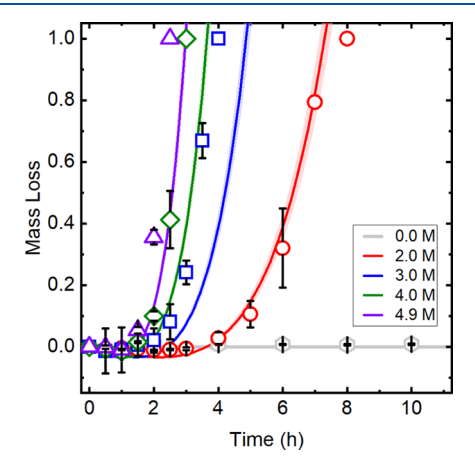


Figure 4. Higher concentration of thiol in the degrading solution led to faster mass loss. Mass loss plotted versus time shows model predictions (lines with error bands) and experimental data (markers with error bars) matched well for BMP concentrations ranging from 0.0 to 4.9 M. Rate constant value used for the model fit was $k = 0.0042 \pm 0.0001 \,\mathrm{M}^{-1} \,\mathrm{min}^{-1}$ including standard error. Error bands on model predictions are error-propagated from standard error on k, and error bars on experimental data are standard deviation.

the initial concentration of free thiol BMP, which ranged from 0.0 to 4.9 M, at a constant ratio of 30 mol % TEA. The 0.0 M sample served as a control with no free thiol added but TEA was included at a concentration that matched the TEA content of the 2.0 M BMP sample in acetone. As thiol concentration increased, the total time for mass loss decreased from ≈8 to \approx 2.5 h for the 2.0–4.9 M samples. Experimental data matched model predictions well, and as predicted at early degradation times, a small amount of mass gain was experimentally observed. Despite having different concentrations of BMP and thus different degradation times, the 2.0-4.9 M samples all had a Z value of 4 and thus experienced the same net mass loss at the same probability of degradation, P, as shown in Figure 2c. Furthermore, the critical probability at which the total mass loss was achieved, P_c , was 0.67 for all samples (eq 5). These model predictions are useful to determine the degradation conditions required to fully degrade a thioester network after a specific amount of time.

The second-order reaction rate constant k was used as a fitting parameter to compare model predictions with experimental results. As such, k is not a function of thiolate concentration, and all experimental data were fit to a single

value of k. Figure 4 shows that a k value of 0.0042 ± 0.0001 M⁻¹ min⁻¹, including standard error, predicted experimental mass loss well for all of the conditions assessed here. Model predictions for the 3.0-4.9 M samples deviated from experimental results more, likely due to the convolution of the measured reaction rate constant with mass transport limitations of large oligomers diffusing out of the degrading polymer network. Nevertheless, the k value from Figure 4 was similar to the Figure 3b value, 0.0042 versus 0.0051 M⁻¹ min⁻¹, and lies closer to previously reported reaction rate constant values for uncatalyzed thiol-thioester exchange in small-molecule aqueous systems $(k \approx 10^{-5} \text{ M}^{-1} \text{ min}^{-1})^{40}$ than to catalyzed exchange in small-molecule systems ($k \approx 10^3 \text{ M}^{-1}$ min⁻¹). 41,42 This decrease was likely due to the limited mobility of thiolates in polymeric systems and the lack of a polar protic solvent to stabilize thiol-thioester exchange. 1

3.3.2. Ratio of Base Catalyst. As the ratio of base increased, the mass loss rate also increased. Figure 5 shows data for how

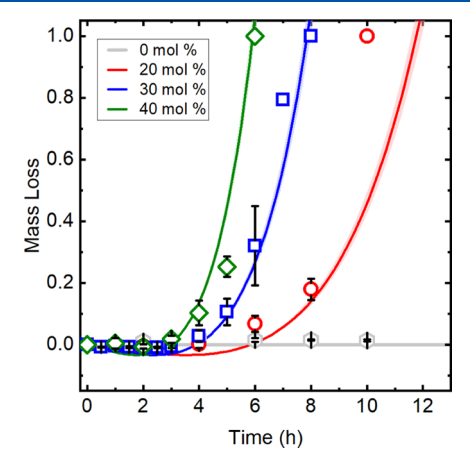


Figure 5. Higher molar ratio of base to thiol in the degrading solution led to faster mass loss. Mass loss plotted versus time shows that model predictions (lines with error bands) and experimental data (markers with error bars) matched well as TEA molar ratio increased from 0 to 40 mol %. Rate constant value used for model fit was $k=0.0039\pm0.0001~\mathrm{M}^{-1}~\mathrm{min}^{-1}$ including standard error. Error bands on model predictions are error-propagated from standard error on k, and error bars on experimental data are standard deviation.

the mass loss changed as a function of the TEA mol ratio, going from 0 to 40 mol %, while keeping the BMP concentration at 2.0 M. The 0 mol % sample served as a control: no TEA was added but 2.0 M BMP in acetone was still included. As the ratio of base to thiol increased from 20 to 40 mol %, the total time for polymer degradation decreased from ≈10 to ≈6 h. Experimental data matched model predictions well, and similar to Figure 4 at early degradation times, a small amount of mass gain was observed. Also similar to Figure 4, even though the 20-40 mol % samples had varying amounts of TEA, all were Z = 4 networks and followed the same net mass loss profile depicted in Figure 2c and achieved total mass loss at $P_c = 0.67$ (eq 5). Lastly, fitting the model prediction to experimental data in Figure 5 resulted in a rate constant k of $0.0039 \pm 0.0001 \text{ M}^{-1} \text{ min}^{-1}$ including standard error, which was similar in value to previous experiments as changing the molar ratio of base catalyst to free thiol should not impact the intrinsic reaction rate constant of thiol-thioester exchange.

3.3.3. Monomer Functionality. Increasing monomer functionality, Z, resulted in slower mass loss. The data in

Figure 6 show how the mass loss changed as a function of Z, where Z ranged from 3 to 6, while using 2.0 M BMP and 30

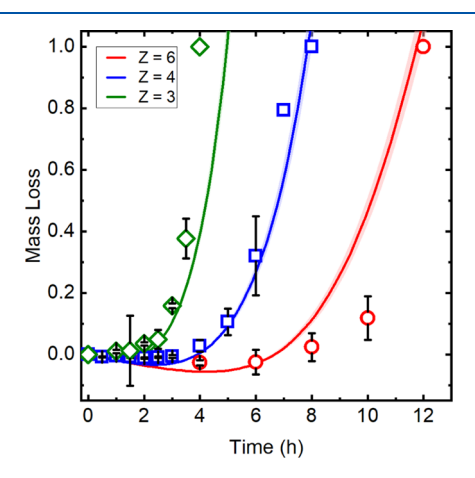


Figure 6. Greater number of functional groups in the network structure led to slower mass loss. Mass loss plotted versus time shows that model predictions (lines with error bands) and experimental data (markers with error bars) matched well for monomer functionality Z when it ranged from 3 to 6. Rate constant value used for model fit was $k=0.0039\pm0.0001~\mathrm{M^{-1}~min^{-1}}$ including standard error. Error bands on model predictions are error-propagated from standard error on k, and error bars on experimental data are standard deviation.

mol % TEA for the degradation solution. Each value of Z came from a different thiol—ene network, where TMPTMP (Z=3), PETMP (Z=4), or diPETMP (Z=6) were reacted with TEDE to make these networks. As Z increased from 3 to 6, the total time for the polymer network to degrade increased from ≈ 4 to ≈ 12 h. Experimental data matched model predictions well, and the Z=6 sample experienced the most mass gain as predicted by the model, reaching approximately 3%.

Unlike Figures 4 and 5, each sample in Figure 6 was modeled by a different mass loss equation, as shown in Figure 2c. As such, each sample had a distinct value of P_c (eq 5): for Z = 3, 4, and 6 P_c equaled 0.5, 0.67, and 0.8, respectively. Larger values of Z resulted in higher P_c values because larger Z networks have a greater number of arms connected to each cross-link, and as such, a higher fraction of thioester groups must cleave before cross-links fully disconnect and a repeat unit leaves the network. Because of this, a Z = 3 network will

achieve greater mass loss than a Z=6 network when the same probability of thioester groups cleaving, P, is reached. Despite the variation in the network structure, the model predictions for all samples yielded a similar value for rate constant k, $0.0039 \pm 0.0001 \, \mathrm{M}^{-1} \, \mathrm{min}^{-1}$, including standard error, suggesting that changes in the polymer network structure had little effect on the reaction rate constant of thiol—thioester exchange.

3.4. 3-D Printing Thioesters. To broaden the scope of these thioester-containing CANs toward industrial applications, SLA 3-D printed thioester networks were investigated. As 3-D printed structures may vary in thickness, and thickness impacts characteristic diffusion time and thus the degradation process, the effect of wall thickness in degrading thioester CANs was studied.

Figure 7a shows model predictions for how time to achieve complete degradation varied with wall thickness when 3-D printed parts were soaked in 2.0 M BMP, 30 mol % TEA degrading solution. Far below the 3 mm wall thickness, bulk degradation dominated as characteristic diffusion time was significantly lower than reaction time. Since bulk degradation occurs simultaneously throughout a polymer network, the time to reach complete degradation was independent of wall thickness and remained a constant 8 h. Far above 3 mm wall thickness, surface degradation dominated as the characteristic reaction time was then significantly lower than the diffusion time. Using the Hopfenberg model, 43 degradation time in the surface degrading regime was predicted to increase linearly with wall thickness, and this rate of increase was driven by the rate of height change of a one dimensional (1-D) polymer slab. Surface degradation carried out on 5 mm thick, 3-D printed slabs of TEDE-PETMP showed height decreases of 0.37 \pm 0.02 mm/h, meaning that in the surface degrading regime degradation time increased with wall thickness at a rate of 2.7 \pm 0.15 h/mm (Figure S5 in the SI). At approximately 3 mm wall thickness, both models converged and network dissolution was a function of both bulk and surface degradation. Following the models described in Figure 7a, one may broaden the design of degradable thioester structures by combining the 3 mm (or other) critical length scale with the two other parameters investigated by this work (i.e., the composition of the degrading solution and the polymer network structure). This approach would enable the creation of multistage degrading 3-D printed networks, where degradation regimes and time

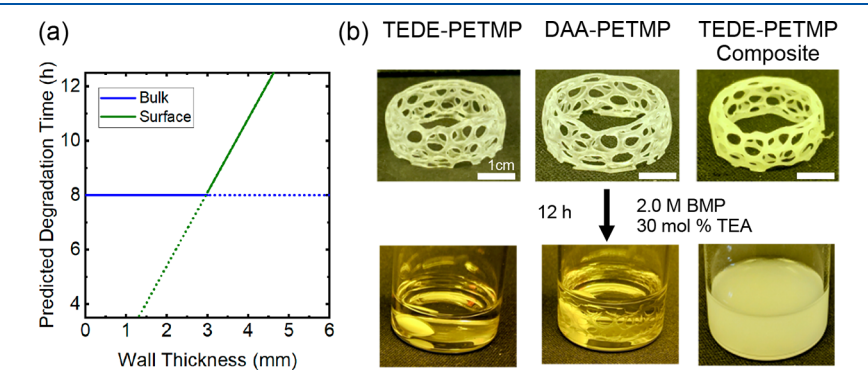


Figure 7. Selective degradation of a thioester network enabled the recovery of fillers in 3-D printed thioester composites. (a) Predicted time for a thioester network to fully degrade plotted versus network thickness, using bulk and surface degradation models. Below 3 mm degradation, time was predicted to be constant. (b) SLA 3-D printed rings composed of various polymer networks (top), with part thickness in the bulk degrading regime, were exposed to a degrading solution (bottom). The TEDE-PETMP composite contained 20 wt % of 6–10 μ m poly(styrene-co-divinylbenzene) microspheres.

scales would be controlled by wall thickness, degradation conditions, and the network structure.

Using the degradation regime predictions from Figure 7a, network dissolution of 3-D printed thioester-containing and 3-D printed thioester-devoid chemistries in the bulk degrading regime was investigated. Voronoi-style lattice rings with strut lengths varying from 0.5 to 2.0 mm and with a consistent strut depth of 0.6 mm were SLA 3-D printed to exhibit the complex structures and rapid production times enabled by additive manufacturing. Since all struts were 0.6 mm deep, this value was used as wall thickness, which was well below the 3 mm threshold and ensured degradation in the bulk degrading regime. Figure 7b shows how the rings, composed of three different networks, behaved after a 12 h soak in the degrading solution previously used for thin film studies (2.0 M BMP, 30 mol % TEA). Networks that contained thioester groups readily dissolved, while networks without the thioester groups were unaffected. Thioester composites containing 20 wt % of 6-10 μm poly(styrene-co-divinylbenzene) microspheres degraded similar to neat networks. Centrifuging the degraded composite solution allowed the recovery of 91 \pm 1.4% of the microspheres, showing efficient recovery of fillers in thioester composites. Unlike composite degradation via other CAN chemistries, thiol-thioester degradation occurred rapidly at room temperature within hours, not days, 44,45 and this dissolution time may be even further reduced through several means such as using a more basic catalyst (diazabicycloundec-7-ene), a more polar solvent (methanol), a more reactive monothiol (methyl thioglycolate), a lower Z monomer (Z =3), or by increasing the temperature of the reaction above room temperature. 16 Beyond this work, one could explore the regions where both reaction and diffusion mechanisms are at play for degradation and how 3-D printed multistage degrading parts may be used to investigate the models developed in this work or other mixed-mode models.^{27,28}

4. CONCLUSIONS

This work investigated degradation kinetics based on thiolthioester exchange for thioester-containing networks. By means of a theoretical model, derived from the reaction kinetics and the polymer network structure, mass gain from the thiol molecules adding into the network and net mass loss from cross-link cleaving were predicted and experimentally verified by mass loss studies. Reaction rate constants, k, used as a fitting parameter for the derived model were found to range from 0.0039 to 0.0051 M⁻¹ min⁻¹ and fit within previously reported values. Further investigations on exchange kinetics and network structure found that increasing the concentration of free thiol, the ratio of base to thiol, or decreasing monomer functionality sped up the mass loss rate. Lastly, SLA 3-D printed thioester composites showed that thioester-containing CANs selectively degraded to allow the recovery of 91% of the filler in a composite, paving the way for thioester-facilitated filler recovery.

Beyond the degradation of thioester-containing CANs, the work herein expands the general understanding of dynamic bond-exchange-based bulk degradation and the use of thermosetting polymers for material recovery. The model derived in this work presents a new method to account for mass gain due to reversible exchange during degradation and is anticipated to be applicable to various dynamic chemistries and CAN applications. The presented procedure to degrade 3-D printed composites establishes a new method to create

degradable thermoset composites and controllably recover fillers from these thermosets on an industrial scale. Altogether, this work shows the versatility of CANs for selective degradation and material recovery applications.

ASSOCIATED CONTENT

Supporting Information

The Supporting Information is available free of charge at https://pubs.acs.org/doi/10.1021/acs.macromol.1c02459.

Derivations to model molecular weight between crosslinks, concentration of thiolate, surface degradation, mass gain, and mass loss; 3-D printing parameters; mass swelling ratio; degradation procedure; and control experiments (PDF)

AUTHOR INFORMATION

Corresponding Author

Christopher N. Bowman — Department of Chemical and Biological Engineering, University of Colorado Boulder, Boulder, Colorado 80309, United States; Materials Science and Engineering Program, University of Colorado Boulder, Boulder, Colorado 80309, United States; orcid.org/0000-0001-8458-7723; Email: christopher.bowman@colorado.edu

Authors

- Juan J. Hernandez Department of Chemical and Biological Engineering, University of Colorado Boulder, Boulder, Colorado 80309, United States; orcid.org/0000-0003-0040-0904
- Adam L. Dobson Department of Chemical and Biological Engineering, University of Colorado Boulder, Boulder, Colorado 80309, United States
- Benjamin J. Carberry Department of Chemical and Biological Engineering, University of Colorado Boulder, Boulder, Colorado 80309, United States; The Bio Frontiers Institute, University of Colorado Boulder, Boulder, Colorado 80309, United States
- Alexa S. Kuenstler Department of Chemical and Biological Engineering, University of Colorado Boulder, Boulder, Colorado 80309, United States; orcid.org/0000-0003-0432-2173
- Parag K. Shah Department of Chemical and Biological Engineering, University of Colorado Boulder, Boulder, Colorado 80309, United States
- Kristi S. Anseth Department of Chemical and Biological Engineering, University of Colorado Boulder, Boulder, Colorado 80309, United States; The Bio Frontiers Institute, University of Colorado Boulder, Boulder, Colorado 80309, United States; orcid.org/0000-0002-5725-5691
- Timothy J. White Department of Chemical and Biological Engineering, University of Colorado Boulder, Boulder, Colorado 80309, United States; Materials Science and Engineering Program, University of Colorado Boulder, Boulder, Colorado 80309, United States; orcid.org/0000-0001-8006-7173

Complete contact information is available at: https://pubs.acs.org/10.1021/acs.macromol.1c02459

Notes

The authors declare the following competing financial interest(s): C.N.B. is an inventor on patents that address

reversible polymerization of thioester-anhydride containing materials and has potential to receive royalties from these patents.

ACKNOWLEDGMENTS

This work was made possible by funding from the Graduate Assistance in Areas of National Need (GAANN) and a National Science Foundation's Grant DMR 1809841. A.S.K. acknowledges support from an Arnold O. Beckman Post-doctoral Fellowship.

REFERENCES

- (1) Barnes, D. K. A.; Galgani, F.; Thompson, R. C.; Barlaz, M. Accumulation and Fragmentation of Plastic Debris in Global Environments. *Philos. Trans. R. Soc., B* **2009**, *364*, 1985–1998.
- (2) Pickering, S. J. Recycling Technologies for Thermoset Composite Materials-Current Status. *Composites, Part A* **2006**, 37, 1206–1215.
- (3) Kloxin, C. J.; Bowman, C. N. Covalent Adaptable Networks: Smart, Reconfigurable and Responsive Network Systems. *Chem. Soc. Rev.* **2013**, *42*, 7161–7173.
- (4) Podgórski, M.; Fairbanks, B. D.; Kirkpatrick, B. E.; McBride, M.; Martinez, A.; Dobson, A.; Bongiardina, N. J.; Bowman, C. N. Toward Stimuli-Responsive Dynamic Thermosets through Continuous Development and Improvements in Covalent Adaptable Networks (CANs). *Adv. Mater.* **2020**, *32*, No. 1906876.
- (5) Nimmo, C. M.; Owen, S. C.; Shoichet, M. S. Diels-Alder Click Cross-Linked Hyaluronic Acid Hydrogels for Tissue Engineering. *Biomacromolecules* **2011**, *12*, 824–830.
- (6) Chao, A.; Negulescu, I.; Zhang, D. Dynamic Covalent Polymer Networks Based on Degenerative Imine Bond Exchange: Tuning the Malleability and Self-Healing Properties by Solvent. *Macromolecules* **2016**, *49*, 6277–6284.
- (7) Kuang, X.; Zhou, Y.; Shi, Q.; Wang, T.; Qi, H. J. Recycling of Epoxy Thermoset and Composites via Good Solvent Assisted and Small Molecules Participated Exchange Reactions. ACS Sustainable Chem. Eng. 2018, 6, 9189–9197.
- (8) Wang, C.; Goldman, T. M.; Worrell, B. T.; McBride, M. K.; Alim, M. D.; Bowman, C. N. Recyclable and Repolymerizable Thiol-X Photopolymers. *Mater. Horiz.* **2018**, *5*, 1042–1046.
- (9) Melchor Bañales, A. J.; Larsen, M. B. Thermal Guanidine Metathesis for Covalent Adaptable Networks. *ACS Macro Lett.* **2020**, 9, 937–943.
- (10) Shi, Q.; Yu, K.; Kuang, X.; Mu, X.; Dunn, C. K.; Dunn, M. L.; Wang, T.; Jerry Qi, H. Recyclable 3D Printing of Vitrimer Epoxy. *Mater. Horiz.* **2017**, *4*, 598–607.
- (11) Yu, K.; Xin, A.; Du, H.; Li, Y.; Wang, Q. Additive Manufacturing of Self-Healing Elastomers. *NPG Asia Mater.* **2019**, 11, No. 7.
- (12) Li, X.; Yu, R.; He, Y.; Zhang, Y.; Yang, X.; Zhao, X.; Huang, W. Self-Healing Polyurethane Elastomers Based on a Disulfide Bond by Digital Light Processing 3D Printing. ACS Macro Lett. **2019**, *8*, 1511–1516.
- (13) Bagheri, A.; Ling, H.; Bainbridge, C. W. A.; Jin, J. Living Polymer Networks Based on a RAFT Cross-Linker: Toward 3D and 4D Printing Applications. *ACS Appl. Polym. Mater.* **2021**, *3*, 2921–2930.
- (14) Göpferich, A. Mechanisms of Polymer Degradation and Erosion. In *The Biomaterials: Silver Jubilee Compendium*; 1996; Vol. 39, pp 117–128.
- (15) Burkersroda, F. Von.; Schedl, L.; Göpferich, A. Why Degradable Polymers Undergo Surface Erosion or Bulk Erosion. *Biomaterials* **2002**, 23, 4221–4231.
- (16) Worrell, B. T.; Mavila, S.; Wang, C.; Kontour, T. M.; Lim, C. H.; McBride, M. K.; Musgrave, C. B.; Shoemaker, R.; Bowman, C. N. A User's Guide to the Thiol-Thioester Exchange in Organic Media: Scope, Limitations, and Applications in Material Science. *Polym. Chem.* **2018**, *9*, 4523–4534.

- (17) Ishibashi, J. S. A.; Kalow, J. A. Vitrimeric Silicone Elastomers Enabled by Dynamic Meldrum's Acid-Derived Cross-Links. *ACS Macro Lett.* **2018**, *7*, 482–486.
- (18) El-Zaatari, B. M.; Ishibashi, J. S. A.; Kalow, J. A. Cross-Linker Control of Vitrimer Flow. *Polym. Chem.* **2020**, *11*, 5339–5345.
- (19) Fairbanks, B. D.; Scott, T. F.; Kloxin, C. J.; Anseth, K. S.; Bowman, C. N. Thiol-Yne Photopolymerizations: Novel Mechanism, Kinetics, and Step-Growth Formation of Highly Cross-Linked Networks. *Macromolecules* **2009**, *42*, 211–217.
- (20) Van Herck, N.; Maes, D.; Unal, K.; Guerre, M.; Winne, J. M.; Du Prez, F. E. Covalent Adaptable Networks with Tunable Exchange Rates Based on Reversible Thiol—Yne Cross-Linking. *Angew. Chem., Int. Ed.* **2020**, *59*, 3609—3617.
- (21) Ghobril, C.; Charoen, K.; Rodriguez, E. K.; Nazarian, A.; Grinstaff, M. W. A Dendritic Thioester Hydrogel Based on Thiol-Thioester Exchange as a Dissolvable Sealant System for Wound Closure. *Angew. Chem., Int. Ed.* **2013**, *52*, 14070–14074.
- (22) Pietrocola, F.; Galluzzi, L.; Bravo-San Pedro, J. M.; Madeo, F.; Kroemer, G. Acetyl Coenzyme A: A Central Metabolite and Second Messenger. *Cell Metab.* **2015**, *21*, 805–821.
- (23) Carberry, B. J.; Hergert, J. E.; Yavitt, F. M.; Hernandez, J. J.; Speckl, K. F.; Bowman, C. N.; McLeod, R. R.; Anseth, K. S. 3D Printing of Sacrificial Thioester Elastomers Using Digital Light Processing for Templating 3D Organoid Structures in Soft Biomatrices. *Biofabrication* 2021, 13, No. 044104.
- (24) Podgórski, M.; Huang, S.; Bowman, C. N. Additive Manufacture of Dynamic Thiol-Ene Networks Incorporating Anhydride-Derived Reversible Thioester Links. ACS Appl. Mater. Interfaces 2021, 13, 12789–12796.
- (25) Yu, K.; Yang, H.; Dao, B. H.; Shi, Q.; Yakacki, C. M. Dissolution of Covalent Adaptable Network Polymers in Organic Solvent. *J. Mech. Phys. Solids* **2017**, *109*, 78–94.
- (26) Kuang, X.; Shi, Q.; Zhou, Y.; Zhao, Z.; Wang, T.; Qi, H. J. Dissolution of Epoxy Thermosets: Via Mild Alcoholysis: The Mechanism and Kinetics Study. *RSC Adv.* **2018**, *8*, 1493–1502.
- (27) Hamel, C. M.; Kuang, X.; Chen, K.; Qi, H. J. Reaction-Diffusion Model for Thermosetting Polymer Dissolution through Exchange Reactions Assisted by Small-Molecule Solvents. *Macromolecules* **2019**, *52*, 3636–3645.
- (28) Marco-Dufort, B.; Willi, J.; Vielba-Gomez, F.; Gatti, F.; Tibbitt, M. W. Environment Controls Biomolecule Release from Dynamic Covalent Hydrogels. *Biomacromolecules* **2021**, *22*, 146–157.
- (29) Metters, A. T.; Bowman, C. N.; Anseth, K. S. A Statistical Kinetic Model for the Bulk Degradation of PLA-b-PEG-b-PLA Hydrogel Networks. *J. Phys. Chem. B* **2000**, *104*, 7043–7049.
- (30) Martens, P.; Metters, A. T.; Anseth, K. S.; Bowman, C. N. A Generalized Bulk-Degradation Model for Hydrogel Networks Formed from Multivinyl Cross-Linking Molecules. *J. Phys. Chem. B* **2001**, *105*, 5131–5138.
- (31) Metters, A.; Hubbell, J. Network Formation and Degradation Behavior of Hydrogels Formed by Michael-Type Addition Reactions. *Biomacromolecules* **2005**, *6*, 290–301.
- (32) Rydholm, A. E.; Reddy, S. K.; Anseth, K. S.; Bowman, C. N. Development and Characterization of Degradable Thiol-Allyl Ether Photopolymers. *Polymer* **2007**, *48*, 4589–4600.
- (33) Shih, H.; Lin, C. C. Cross-Linking and Degradation of Step-Growth Hydrogels Formed by Thiol-Ene Photoclick Chemistry. *Biomacromolecules* **2012**, *13*, 2003–2012.
- (34) Worrell, B. T.; McBride, M. K.; Lyon, G. B.; Cox, L. M.; Wang, C.; Mavila, S.; Lim, C. H.; Coley, H. M.; Musgrave, C. B.; Ding, Y.; Bowman, C. N. Bistable and Photoswitchable States of Matter. *Nat. Commun.* **2018**, *9*, No. 2804.
- (35) Long, T. R.; Elder, R. M.; Bain, E. D.; Masser, K. A.; Sirk, T. W.; Yu, J. H.; Knorr, D. B.; Lenhart, J. L. Influence of Molecular Weight between Crosslinks on the Mechanical Properties of Polymers Formed: Via Ring-Opening Metathesis. *Soft Matter* **2018**, *14*, 3344–3360.

- (36) Macosko, C. W.; Miller, D. R. A New Derivation of Average Molecular Weights of Nonlinear Polymers. *Macromolecules* **1976**, *9*, 199–206.
- (37) Hiemenz, P. C.; Lodge, T. P. Polymer Chemistry, 2nd ed.; CRC Press Taylor & Francis Group, 2007.
- (38) Flory, P. J. Molecular Size Distribution in Three Dimensional Polymers. I. Gelation1. *J. Am. Chem. Soc.* **1941**, *63*, 3083–3090.
- (39) Chen, J. S.; Ober, C. K.; Poliks, M. D.; Zhang, Y.; Wiesner, U.; Cohen, C. Controlled Degradation of Epoxy Networks: Analysis of Crosslink Density and Glass Transition Temperature Changes in Thermally Reworkable Thermosets. *Polymer* **2004**, *45*, 1939–1950.
- (40) Cargoët, M.; Diemer, V.; Snella, B.; Desmet, R.; Blanpain, A.; Drobecq, H.; Agouridas, V.; Melnyk, O. Catalysis of Thiol-Thioester Exchange by Water-Soluble Alkyldiselenols Applied to the Synthesis of Peptide Thioesters and SEA-Mediated Ligation. *J. Org. Chem.* **2018**, *83*, 12584–12594.
- (41) Bracher, P. J.; Snyder, P. W.; Bohall, B. R.; Whitesides, G. M. The Relative Rates of Thiol-Thioester Exchange and Hydrolysis for Alkyl and Aryl Thioalkanoates in Water. *Orig. Life Evol. Biosph.* **2011**, 41, 399–412.
- (42) Um, I. H.; Lee, J. Y.; Bae, S. Y.; Buncel, E. Effect of Modification of the Electrophilic Center on the α Effect. *Can. J. Chem.* **2005**, 83, 1365–1371.
- (43) Hopfenberg, H. B. Controlled Release from Erodible Slabs, Cylinders, and Spheres. In ACS Symposium Series, 1976; Vol. 33, pp 26–32.
- (44) Yu, K.; Shi, Q.; Dunn, M. L.; Wang, T.; Qi, H. J. Carbon Fiber Reinforced Thermoset Composite with Near 100% Recyclability. *Adv. Funct. Mater.* **2016**, *26*, 6098–6106.
- (45) Taynton, P.; Ni, H.; Zhu, C.; Yu, K.; Loob, S.; Jin, Y.; Qi, H. J.; Zhang, W. Repairable Woven Carbon Fiber Composites with Full Recyclability Enabled by Malleable Polyimine Networks. *Adv. Mater.* **2016**, *28*, 2904–2909.

Recommended by ACS

Synthesis of Poly(glycerol butenedioate)—PGB—Unsaturated Polyester toward Biomedical Applications

Michał Wrzecionek, Agnieszka Gadomska-Gajadhur, et al.

JULY 15, 2022 ACS OMEGA

READ 🗖

Synthesis of Bio-Based Photo-Cross-Linkable Polyesters Based on Caffeic Acid through Selective Lipase-Catalyzed Polymerization

Alfred Bazin, Eric Pollet, et al.

MAY 24, 2022

MACROMOLECULES

READ **M**

Construction and Synthesis of High-Stability Biobased Oligomeric Lactate Plasticizer: Applicable to PVC and PLA Polymers

Zheming Zhang, Jie Pan, et al.

AUGUST 25, 2022

INDUSTRIAL & ENGINEERING CHEMISTRY RESEARCH

READ **M**

Toward Sustainable Elastomers from the Grafting-Through Polymerization of Lactone-Containing Polyester Macromonomers

Lucie Fournier, Marc A. Hillmyer, et al.

JANUARY 19, 2022

MACROMOLECULES

READ **M**

Get More Suggestions >